Nanorotors and self-assembling macromolecular machines: the torque ring of the bacterial flagellar motor

Daniela Stock[1,2], Keiichi Namba[3,4] and Lawrence K Lee[1,2]

The bacterial flagellar motor (BFM) is a self-assembling rotary nanomachine. It converts a flux of cations into the mechanical rotation of long filaments that propel bacteria through viscous media. The BFM contains a torque-generating ring that is complete with molecular machinery known as the switch complex that allows it to reverse directions. With four billion years of optimization, the BFM probably offers the pinnacle of sophisticated nanorotor design. Moreover as one of the best-characterized large biomolecular complexes, it offers the potential for convergence between nanotechnology and biology, which requires an atomic level understanding of BFM structure and function. This review focuses on current molecular models of the reversible BFM and the strategies used to derive them.

Addresses
[1] Structural and Computational Biology Division, The Victor Chang Cardiac Research Institute, Lowy Packer Building, 405 Liverpool St, Darlinghurst, NSW 2010, Australia
[2] The University of New South Wales, Sydney, NSW 2052, Australia
[3] Graduate School of Frontier Biosciences, Osaka University, 1-3 Yamadaoka, Suita, Osaka 565-0871, Japan
[4] Riken Quantitative Biology Center, 1-3 Yamadaoka, Suita, Osaka 565-0871, Japan

Corresponding author: Lee, Lawrence K (l.lee@victorchang.edu.au)

Introduction
Architecture of the bacterial flagellar motor
The architecture of the BFM in *Salmonella sp.* has been revealed in considerable detail with single particle electron microscopy (EM) [1,2]. The subcomplex that is responsible for torque generation and motor reversal is comprised of four proteins in the rotor component FliF, FliG, FliM and FliN; and two proteins MotA and MotB in the stator component. FliF alone forms a 26-fold ring (MS-ring) of 24 nm diameter [2], whereas in an intact BFM, the MS-ring crosses the inner membrane and forms a ∼30 nm ring [1]. The MS-ring is one of the first substructures to form and acts as a scaffold for the assembly of the rest of the BFM [3,4,5••]. Next in the assembly line is

the switch complex, which contains dozens of copies of FliG, FliM and FliN. This assembles at the base of the MS-ring where it forms a large bell-like ring of ∼45 nm diameter known as the C-ring (Figure 1).

The MotAB stator complexes (PomAB in sodium dependent motors) cross the cytosolic membrane to form the ion channels that mediate an influx of protons or sodium ions, providing the energy for torque generation. High-resolution structures of periplasmic fragments of MotB [6,7] and the architecture of an intact PomAB stator were recently elucidated [8•] (Figure 1). As stators readily dissociate from non-rotating motors [4] these are not seen in EM micrographs of isolated basal bodies. However advances in electron cryotomography (ECT) have allowed the visualization of intact BFM structures *in situ* [9,10]. Three recent *in situ* ECT studies improved the resolution of 3D maps obtained from the first *in situ* BFM images [11] and corroborate the finding that the MotAB stators are positioned on the outside of the MS-ring, in contact with the outer periphery of the C-ring [12•,13•,14] (Figure 1).

The switch complex
The switch complex is the rotor component responsible for torque generation and motor reversal. FliG is the rotor protein most directly involved in torque generation and hence motor switching. Charged residues on or around a single helix (torque helix) in the C-terminal domain interact directly with at least two residues on the stator protein MotA to generate torque [15–19]. And it is thought that rotational switching is a result of a reorientation of this torque helix [20••,21,22,23••]. FliM and FliN are situated in the C-ring [24] but the location of FliG remains contentious. FliG appears to be present in BFMs where the C-ring is removed [24,25] suggesting that FliG lies on the cytoplasmic face of the MS-ring [25]. However, a 3D EM reconstruction of a FliF–FliG fusion protein ring revealed only a relatively small volume of additional density over FliF alone on the outer periphery of the M-ring [2], indicating that a large part of FliG might be disordered in the absence of FliM and FliN and therefore not visible in EM. Moreover, MotAB stators do not appear to be in contact with the cytoplasmic face of the MS-ring, but rather with the outer lobe of the C-ring (Figure 1) suggesting that the FliG C-terminal domain is on the outer lobe of the C-ring.

It is thought that a conformational change in FliG reorients the torque helix and results in a switch from its default counter clockwise (CCW) to a clockwise (CW)

Figure 1
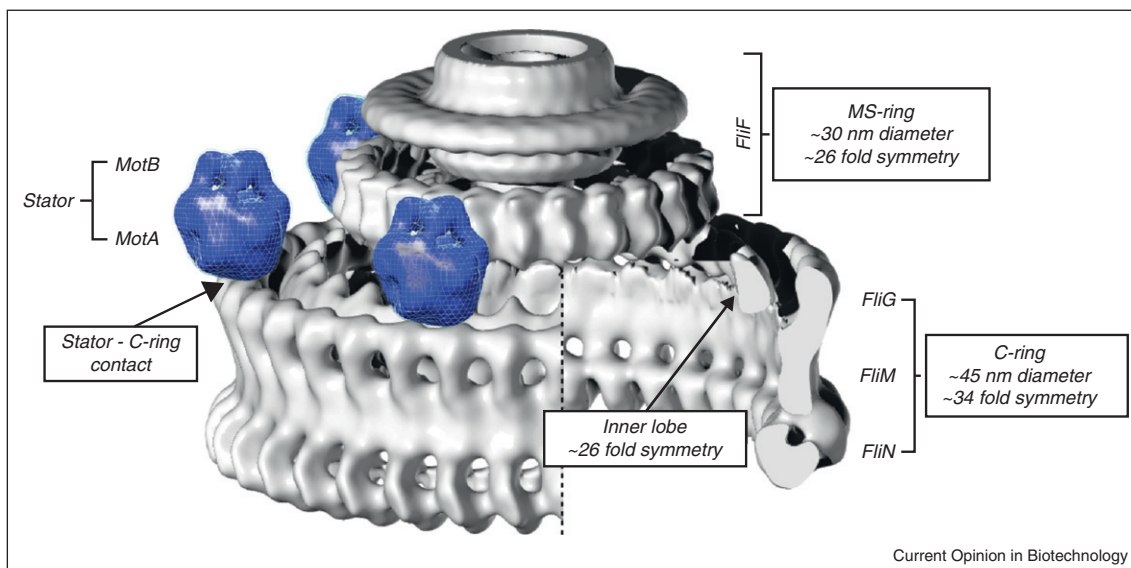
Architecture of the bacterial flagellar motor. A 3D EM reconstruction of the CW-locked motor from *Salmonella typhimurium* (EMDB accession code: 1887) [1] is displayed, rendered in gray. A 3D EM reconstruction of the PomAB stator complex is shown in blue and positioned above the outer lobe of the C-ring where it is seen in electron cryotomograms. Images of the PomAB stator are adapted from Yonekura *et al.*, 2011 [8•].

rotational state in *S. typhimurium* and *E. coli*, which alters the trajectory of swimming bacteria. FliM and FliN on the contrary induce this conformational change in response to an interaction with a phosphorylated chemotactic protein known as CheY-P; the end point of a well-studied sensory network that facilitates bacterial chemotaxis [26•]. In addition, other novel control mechanisms have been revealed, which were recently reviewed [27•]. The BFM switch is highly cooperative with protomers favoring being either all in a CW or CCW rotational state [28,29] and has a very steep dependence on CheY-P concentration with a calculated Hill coefficient of ∼10.3 [30]. Importantly however, *in vivo* FRET revealed that CheY-P binding is much less cooperative (Hill coefficient of ∼1.8) [31], indicating that BFM switching is not tightly coupled to CheY-P binding. This suggests that the cooperative machinery is intrinsically tied into the molecular arrangement of the switch complex.

### The symmetry mismatch conundrum
The location of FliG in the outer lobe of density leads to an unsolved conundrum; this lobe contains a ∼34-fold rotational symmetry but several lines of evidence suggest that there are ∼26 FliG molecules. BFMs comprised of a FliF–FliG fusion protein are motile [25], indicating that FliG and FliF, which forms a ∼26-fold ring [2] exist in a 1:1 stoichiometry. In addition, 26 equal substeps per cycle are detected during rotation [32••,33]. Combined, these data suggest that there should be ∼26 copies of FliG to match the 26-fold symmetry in the FliF MS-ring. Importantly however, there may not be a strict requirement for a

particular FliG:FliF stoichiometry as C-rings of a range of sizes with symmetries of 31–38 are observed without a corresponding increase in MS-ring size [34]. This finding is supported by a recent ECT study performed on BFMs from many phylogenetically diverse bacteria. The study demonstrates that while the MS-ring is remarkably conserved in size and shape, C-ring diameters vary dramatically from 34 to 57 nm [35••]. Thus although a 1:1 FliF:FliG stoichiometry is compatible with functional motors in *Salmonella*, significantly different stoichiometries are also likely to be possible.

Towards an atomic model of the FliG torque ring and switch complex
At present, there are no atomic scale pictures of functional BFM subcomplexes. Thus to build an atomic scale model of a functional switch complex, it is necessary to unify the plethora of biochemical and biophysical data collected over the past few decades. This is similar to Watson and Crick's approach to the DNA structure and Pauling's to the alpha helix. However rather than relatively simple purine or pyrimidine bases, the pieces of this puzzle come from high-resolution protein structures, which are complicated dynamic molecular machines in their own right. In addition to the structures of FliG, FliM and FliN fragments [36–38], three new puzzle pieces have recently been reported. These are high-resolution structures of the full-length FliG protein [20••], the middle domain of FliM bound to the middle domain of FliG (FliGm–FliMm) [39••] and a structure of a CW-locked fragment of FliG [22] (Figure 2). All structures have provided

Figure 2
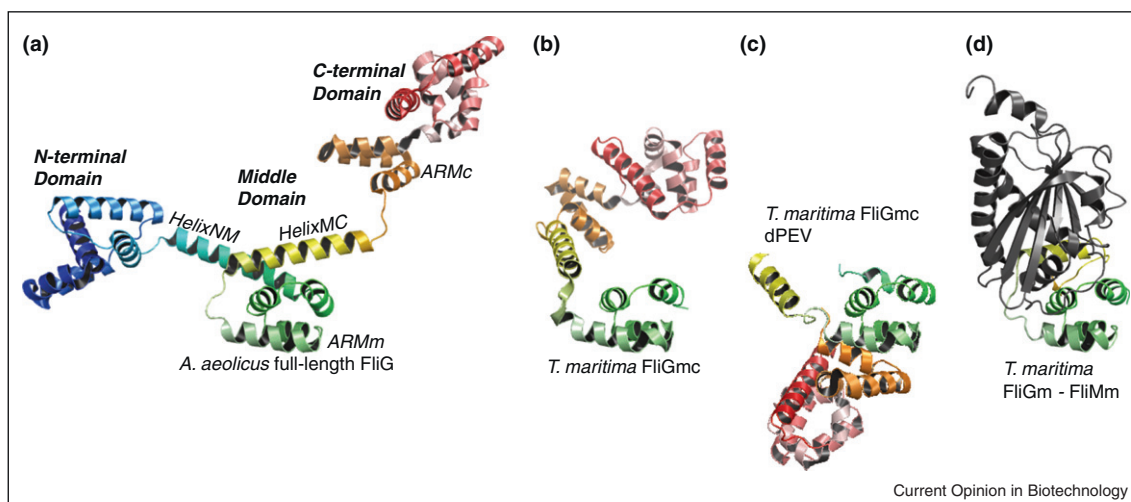
High-resolution X-ray structures of **(a)** full-length FliG from *A. aeolicus*, **(b)** FliG middle and C-terminal domain (FliGmc) from *T. maritima*, **(c)** a CW-locked FliGmc from *T. maritima* and **(d)** the middle domain of FliG (FliGm) in complex with the middle domain of FliM (FliGm) from *T. maritima*. Backbone traces are depicted in cartoon format with equivalent residues colored the same. Structures are shown with FliGm in the same orientation. Structural motifs are labeled in **(a)** only.

important additional clues to the atomic structures of the FliG torque-ring and switch complex. These have resulted in three apparently incompatible models of the FliG ring, which were derived in very different ways. This review examines some of their merits and limitations and the strategies employed to build atomic models of this sophisticated macromolecular machine.

Current molecular models of the BFM torque ring
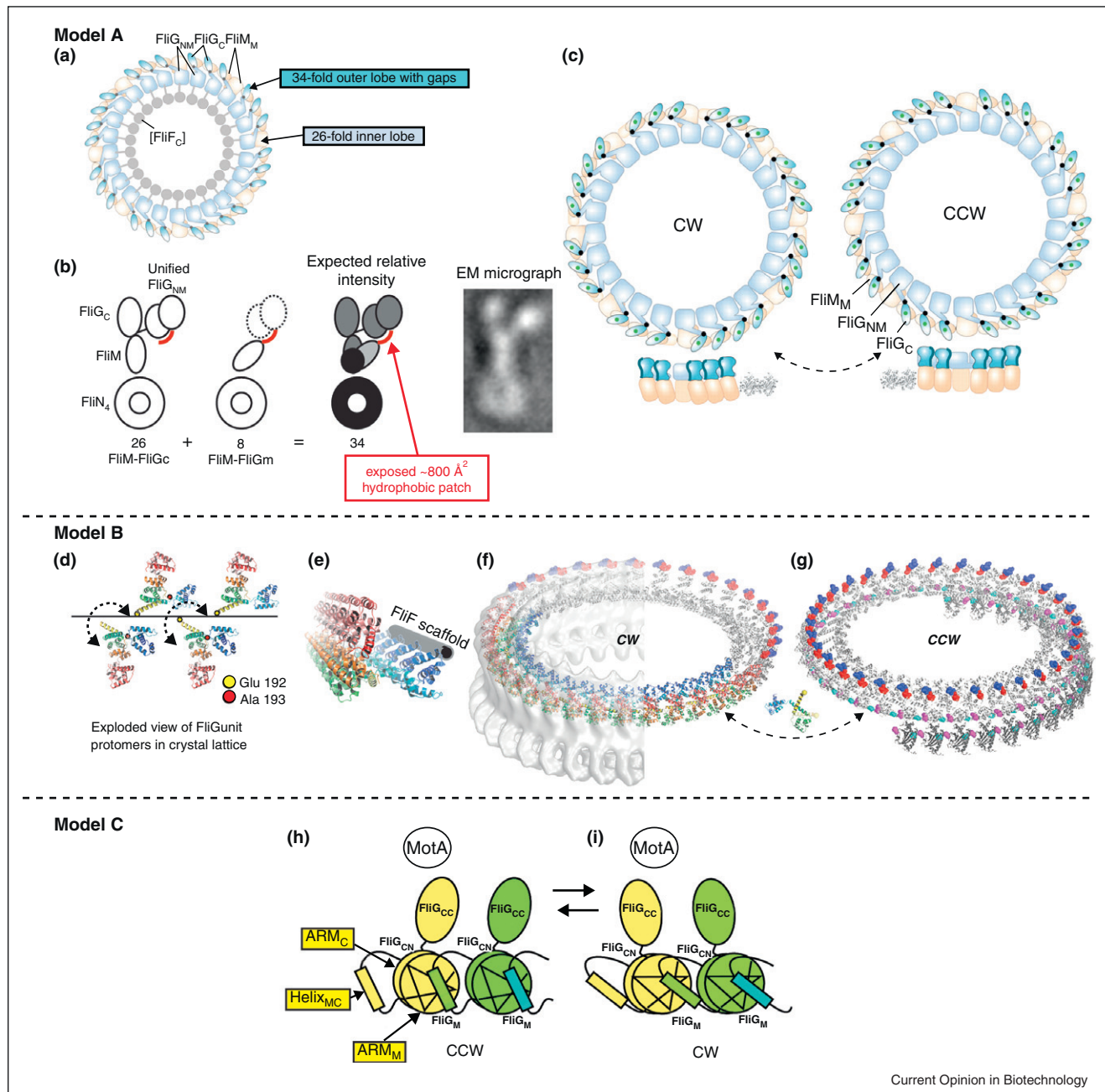### Model A

The most prominent model (Model A) in the literature was constructed by arranging high-resolution X-ray structures of FliG to fit with biochemical and EM experiments [23[••],39[••],40,41,42[•]]. Although the model was first proposed in 2007 [40] subunit arrangement is more or less unchanged, but presented in the context of the recent FliGm–FliMm crystal structure (Figure 2D) and additional cross-linking experiments [39[••]] to include a molecular model for rotational switching [23[••],42[•],43[••]]. Model A was the first to suggest that FliG is in the inner and outer lobe of the C-ring, with the C-terminal domain (FliGc) forming the outer lobe. The inner lobe consists of the N-terminal two-thirds of the protein, which are modeled as a single 'unified' globular domain referred to as FliGnm [39[••]] (Figure 3). To account for the symmetry mismatch between the inner and outer lobe of density, an interesting arrangement of 26 FliG subunits is proposed. The 34-fold symmetry in the outer lobe is accounted for as follows. While FliGc is in a position corresponding to the outer lobe of density, there are only 26 subunits. These are aligned above 34-FliM molecules, with a gap every fourth or fifth molecule (Figure 3A). Thus, apart

from the gaps, intersubunit spacing of FliGc corresponds to the distance of a 34-fold repeat. It is suggested that gaps in the outer lobes would not be observable in 3D EM reconstructions since these densities are invariably averaged [39[••],41].

FliGc is oriented with its torque helix proximal to the membrane where an interaction with the MotA stator occurs, and its base adjacent to the wall of the C-ring where FliM is expected to be. FliM is modeled bound to the base of FliGc, in keeping with biochemical evidence [39[••],40,44,45]. In addition, a conserved EHPQ sequence in the middle domain of FliG (FliGm) also interacts with FliM. A distinguishing feature of this model is that FliG has two distinct FliM binding sites. It is proposed that all 26 FliGcs are bound to 26 FliM monomers. The remaining eight FliM monomers are slanted inwards and occupy a binding site on FliGm (Figure 3B).

This arrangement of FliG monomers roughly reflects the architecture of the BFM as determined by 3D EM reconstructions. But there are notable inconsistencies. First, although the size and shape of the EM density on the outer lobe of the C-ring complements the high-resolution structure well, the proposed gaps should be discernable even in averaged EM density. The gaps would result in outer lobe EM density that is roughly two-thirds (26FliGs/34FliMs) intensity than in the rest of the C-ring (Figure 3B). This is not the case; the outer lobe intensity is roughly the same as the wall and the base of the C-ring. Furthermore, the gaps are not in agreement with the 26 equal steps per revolution [32[••],33]. Second, the eight slanting FliM monomers should similarly be

Figure 3

Three recent models of the FliG torque ring and switch complex. The proposed subunit organization of FliF, FliG and FliM in Model A is depicted schematically in **(a)** gaps in the outer periphery account for the symmetry mismatch between the inner and outer lobe of the C-ring. This results in two different FliG/FliM/FliN arrangements that are suggested to occur in the same ring. These are shown schematically in **(b)** along with an expected resulting density distribution and EM micrograph of a vertical cross-section of a WT BFM C-ring. The approximate position of an exposed hydrophobic patch is labeled in red. **(c)** Schematic representation of the switch mechanism proposed by Model B. Switching involves the relative rotation of FliM subunits, which are bound to FliGc and subsequently result in a reorientation of the torque generating charges on FliG. **a** and **c** are modified from Paul *et al.* PNAS [23••] and the EM micrograph **(b)** is reproduced from Thomas *et al.*, 2006 [1].Model B was constructed primarily based on high-resolution X-ray data. **(d)** An exploded view of the *A. aeolicus* full-length FliG crystal packing that highlights the orientation of adjacent FliGunits. These are connected by a two-residue Glu-Ala loop that should allow adjacent FliG units to swivel relative to each other. By aligning the N-terminal domains in accordance with the expected position of FliF the relative arrangement of FliG subunits is almost fully defined **(e)**. **(f** and **g)** are resulting FliG rings in CW and CCW rotational states. Charged residues involved in torque generation are highlighted in red (negative) and blue (positive) spheres respectively. Movement of the long helix (helixMC) that mediates the transition between these two states is shown between the rings. The CW ring in **(f)** is shown partially docked into 3D EM density from a CW-locked C-ring (EMDB accession code 1887). In **(g)** a partial FliM ring is shown that was created by superimposing the FliGm domain of the FliGm–FliMm crystal structure onto the CCW ring. Residues pairs that were independently shown

Figure 4
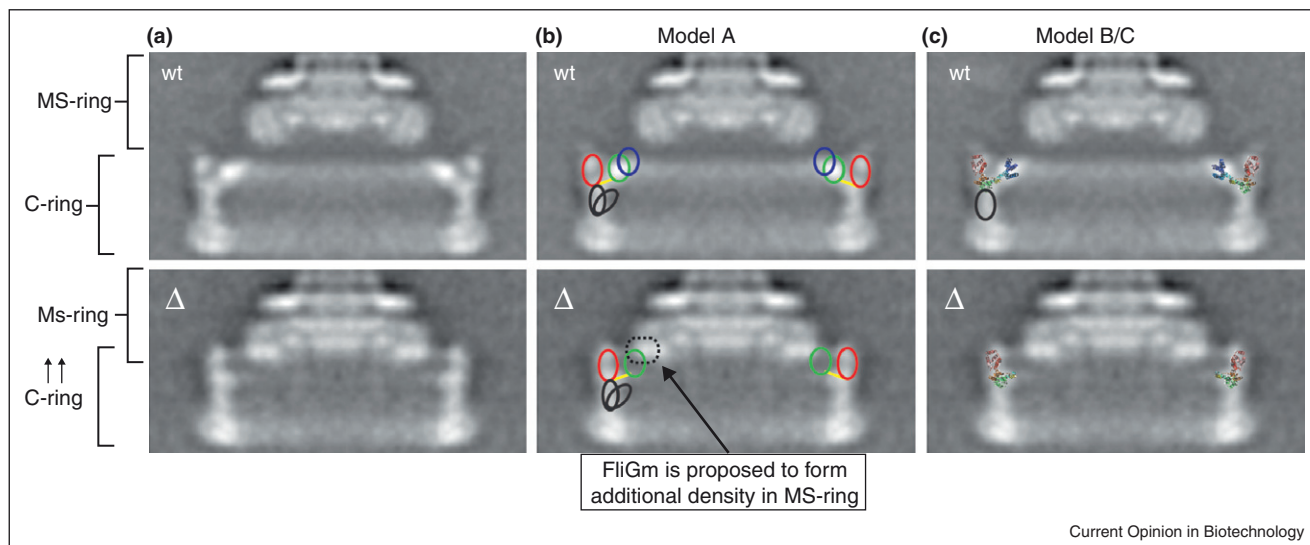
Models of the FliG torque ring compared with electron micrographs of WT (top) and BFMs containing a FliF–FliG fusion deletion mutant from *Salmonella* (bottom). The micrographs are displayed alone **(a)** and overlaid with Model A **(b)** and Model B **(c)**, which is similar to model C. Domains in **(b)** are represented by ovals corresponding to the correct size of FliGc in red, FliGm and FliGn, which form a unified FliGnm domain in green and blue respectively and FliMm in black. In Model A, the FliF–FliG fusion deletion mutant is suggested to result in FliGm moving into the MS-ring where additional density is observed. **(c)** Overlay of the CW-state of Model B. In the FliF–FliG fusion deletion micrograph, the first 94 residues of FliG are deleted from the model to correspond to the missing residues in the fusion deletion mutant. These missing residues correlate well with the missing electron density.

seen in averaged EM densities. Rather than producing an equally distributed intensity in the vertical wall of the C-ring, FliM density should be distributed in a triangular shape where the intensity at the vertices would be significantly different, but EM data show no evidence of this (Figure 3B). Finally, EM micrographs of a FliF–FliG fusion deletion mutant where the C-terminal 56 residues of FliF and the N-terminal 94 residues from FliG are genetically deleted are not well explained by this model. The inner lobe is suggested to contain a unified FliGnm domain. But deletion of what should be half of this putative domain causes the entire lobe to disappear. In addition, the C-ring shifts significantly towards the MS-ring [46] (Figure 4A). It is proposed that FliGm integrates into the base of the MS-ring [39••] (Figure 4B). However it is not clear from the model why either phenomenon would occur (Figure 4).

Aspects of Model A also appear to be at odds with high-resolution structural data. Model A assumes that FliG contains two globular domains. Since this was proposed,

the structure of full-length FliG was elucidated, which revealed three distinct globular domains [20••] (Figure 2A). However, rather than adapting the model, a unified globular FliGnm domain was constructed (Figure 3B) and the topology of the experimentally determined structure was suggested to be an artifact [39••]. In addition, crystal structures of FliGm and FliGc contain a conserved, sizable hydrophobic patch of $\sim$812 and $\sim$851 Å^2 respectively (calculated from the *A. aeolicus* FliG structure). These are unlikely to be exposed to bulk solvent. In Model A, it is possible that the hydrophobic patch on FliGc is shielded by the proposed FliGc–FliM interaction. However, the hydrophobic patch on FliGm remains exposed even when bound to FliM [39••] (Figure 2). Thus, Model A leaves a $\sim$21 000 Å^2 (26 Å $\times$ 812 Å) hydrophobic surface exposed to bulk solvent (Figure 3B).

Model B
Another model of the FliG torque ring was constructed in a very different way. Model B is built from restraints

(**Figure 3 Legend Continued**) to crosslink in targeted cysteine mutagenesis assays are shown as magenta and cyan spheres in both FliG and FliM. Finally, a schematic depiction of Model C is shown in a **(h)** CCW and **(i)** CW rotational state. FliG from the same polypeptide chain are colored the same. The ARMm–ARMc superhelix is proposed to involve an intramolecular interaction. FliG molecules are linked by HelixMC, which extends away from ARMm from its own subunit to bind to its neighbor, then loops back to connect with ARMc. Movement of HelixMC into different conformations is proposed to occur during switching. This results in a reorientation of neighboring FliG subunits and hence provides a mechanism for cooperativity. The schematic depiction of Model C was adapted from Minamino *et al.*, 2011 [22].

almost entirely defined by high-resolution X-ray structures. These restraints are two-fold.

Intra-molecular restraints
Under the assumption that globular folds and secondary structure observed in crystal structures are correct, FliG subunits are only allowed to move around flexible unstructured loops. Thus, the model stays true to the 'puzzle pieces' defined by high-resolution structural data.
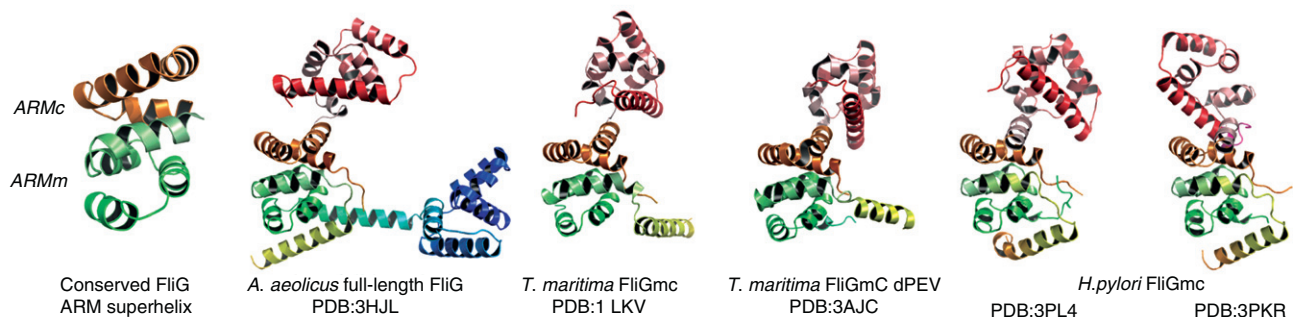
Intermolecular restraints
Based on the argument outlined in Box 1, Model B proposes that an intermolecular FliG–FliG interaction

seen in all FliG crystal structures is biologically relevant. This interaction consists of two three-helix folds known as Armadillo Repeat Motifs [47,48•] (ARM). One of these is at the base of FliGm (ARMm) and the other at the base of FliGc (ARMc) of an adjacent monomer (Figure 2A). The hydrophobic surfaces on FliGm and FliGc constitute a face of ARMm and ARMc respectively. These mediate the ARMm–ARMc interaction and hence each ARM completely shields the other's hydrophobic face from bulk solvent, forming a continuous intermolecular domain consisting of a right-handed super helix (Box 1). One implication of this is that a functional FliG arrangement is a domain swapped, L-shaped FliG protomer (FliGunit) that consists of a

---

Box 1 Biological relevance for FliG Armadillo Repeat Interaction?

β-catenin
PDB:1JDH

SYS-1
PDB:3C2H

Plakophilin
PDB:1XM9

Importin-α
PDB:1BK5
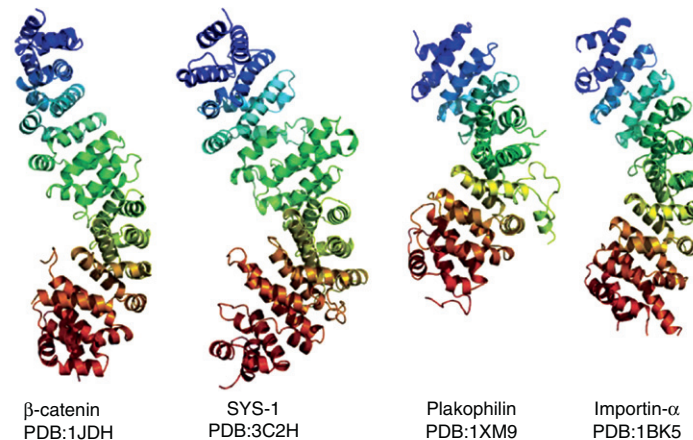
Armadillo Repeat Motifs (ARM) contain ~42 amino acids and form a three-helical fold. They are found in a large family of proteins with diverse functions, some of which have been well characterized in eukaryotes (see Tewari et al for a recent review [43] image above reproduced from [43]). Although their overall sequence identity is not necessarily high, ARMs are structurally well characterised and typically contain a characteristic spread of hydrophobic amino acids, most commonly valine, leucine and isoleucine residues [42]. They have been visualized in dozens of crystal structures from at least 10 different proteins and without exception; these hydrophobic residues mediate specific interactions between tandem ARMs that stack together to form right-handed superhelices.

ARMc

ARMm

Conserved FliG
ARM superhelix

A. aeolicus full-length FliG
PDB:3HJL

T. maritima FliGmc
PDB:1 LKV

T. maritima FliGmC dPEV
PDB:3AJC

H.pylori FliGmc

PDB:3PL4

PDB:3PKR

The FliG ARMs similarly contain a spread of conserved valine, leucine or isoleucine residues, which in all five FliG crystal structures, mediate an identical ARMm-ARMc interaction. However, the FliG ARM superhelix uniquely involves an intermolecular interaction, which raises the possibility that the interaction is a non-specific crystallographic artifact. Indeed, a recent crosslinking experiment did not support a biological role for the ARMm-ARMc interaction [39]. X-ray data argues against this. FliG crystal structures were derived from different species, constructs, crystallization buffers and crystallographic spacegroups with no other conserved intermolecular contacts. As this is unlikely to have occured by chance, it appears that a functional FliG protomer (FliGunit) includes the FliG ARM superhelix in an L-shaped arrangement defined by X-ray crystal structures. FliGunits from all crystal structures are shown above and consist of an N-terminal domain, an ARM superhelix and the C-terminal domain.

Current Opinion in Biotechnology

---

globular N-terminal, ARM superhelix and C-terminal domain (Box 1). Thus, FliG protomers are covalently linked, like beads on a string, where the only degree of freedom is for these beads to swivel relative to each other around a short (2-residue) unstructured loop (Figure 3D). Ensuring that the N-terminal domains of FliG are on the inner circumference of the torque ring where they can bind to FliF strongly restrains this remaining degree of freedom (Figure 3E). Thus Model B suggests that if the crystal structures are correct, there is only one possible arrangement for the FliG torque ring (Figure 3F, G).

This final restraint positions FliGn in the inner lobe of C-ring density with helices involved in binding to FliF pointing towards the MS ring. Like with Model A the torque helix of FliGc is proximal to the membrane. In contrast to Model A, FliGm is bound to the base of FliGc forming the right-handed ARM superhelix (Box 1). Thus both the EHPQ motif and the base of the FliGc are pointing to the wall of the C-ring where FliM is expected to be. Indeed, superimposing the FliGm domain from the FliGm–FliMm structure (Figure 2D) onto the CCW FliG model creates a FliM ring that agrees well with EM density. Moreover, each FliM is oriented such that residues involved in FliM–FliM interactions according to cross-linking studies are in contact (Figure 3G). Importantly, this occurs without any alteration to the CCW FliG model. Similarly, high-resolution structural restraints independently arrange FliG monomers in an orientation that is in agreement with cross-linking studies performed before its construction (Figure 3G), although a subsequent cross-linking study is at odds with the ARM superhelix (Box 1). Finally, adjacent FliG protomers are ~4.11 nm apart at their outer circumference, which is defined by the length and position of helixMC. This is roughly equivalent to the circumference of the C-ring divided into 34 parts (45 nm × π/34 = 4.16 nm). Thus a ~34-fold symmetry in a ~45 nm ring is inherently built into the structure.

It should be noted that a similar analyses concluded that Model B was not consistent with EM data nor the FliGm–FliMm crystal structure [39[••]]. However, these were not performed on the coordinates of model B and are invalid.

The model also explains the EM micrographs of the FliG–FliF fusion deletion mutant well. The N-terminal 94 residues consist of the entire N-terminal domain, which is suggested to form the inner lobe and part of HelixNM, which connects the inner and outer lobe. Thus, deletion of these residues would result in the removal of the inner lobe of density and a shift of the C-ring towards the MS-ring to adjust for the reduced distance between FliF and FliGm (Figure 4C). Despite its agreement with EM, the model does not offer an explanation to the symmetry mismatch between the inner and outer lobe. The current model would locate FliG in the inner lobe, which interacts with FliF, accounting for the 26-fold structural features of the inner lobe. However, Model B is not in agreement with data pointing to a 26-fold FliG stoichiometry nor the 26 equal steps per revolution [32[••],33].

Model C
A third model (Model C Figure 3H, I) was proposed upon the recent elucidation of an additional FliGmc crystal structure (FliGmc-CW), which contained a three amino acid deletion (dPEV) that locks BFMs into CW rotation. This model also proposes that the FliGunit is the functional arrangement of FliG subunits. Thus the overall arrangement and orientation of FliG subunits, and fit with EM density is the same as Model B. The molecular details of Model B and C differ in two ways. The first is in the conformation of the long helix that connects FliGm to FliGc (helixMC – Figure 2A). In Model B helixMC is in close contact with FliGm in the default CCW state, as observed in the WT crystal structure of the full-length protein (Figure 2A). Model C proposes that this interaction does not occur in a physiological context, rather that helixMC is dissociated from FliGm as seen in the crystal structures of FliGmc and FliGmc-CW. Second, that the ARMm–ARMc interaction occurs within the same subunit, which appears to be the case in the CW-locked FliG crystal structure. However, an unresolved connection between ARMm and ARMc in this crystal structure makes this interpretation uncertain. Moreover, these proposed differences require helixMC to extend away from its subunit then double back to FliGc (Figure 3H, I). This is only possible if helixMC is substantially unraveled into an extended loop, and hence is at odds with both FliG WT crystal structures where helixMC is fully resolved as a single straight helix.

Models for rotational switching
Model A
Model A offers the most comprehensive model of rotational switching that extends beyond the FliG ring to the entire switch complex and interactions with CheY-P. Switch-mediated changes that occur to domain interfaces between adjacent FliN [42[•]] and FliM [23[••]] molecules were recently mapped with cross-linking and binding studies. Changes in cross-linking patterns in the presence of chemotactic stimuli indicate that FliN moves relative to the C-terminal domain of FliM (FliMc) and that FliMm rotates relative to its neighbor (Figure 3C). Since in model A, FliM is bound to the base of the FliGc, rotation of FliM should result in a corresponding rotation of the FliGc. This in turn reorients torque-generating charges and results in rotational switching (Figure 3C). The model does not suggest inherent cooperativity within the FliG or FliM ring. Rather, cooperativity is proposed to arise from a spiral-shaped FliN–FliMc ring at the base of the C-ring [23[••]]. In addition, a two-step CheY-P binding mechanism might

also contribute to the cooperativity. In this scheme CheY-P initially binds non-cooperatively to an N-terminal FliM peptide. This serves to recruit CheY-P to the switch complex, but the switch does not occur until a sufficient number of FliM molecules are accumulated to trigger the switch [43[••]].

Model B

Like its subunit arrangement, the switch mechanism in Model B was also determined almost entirely from high-resolution structural data. The essential details are based on a single conformational change involving helixMC. HelixMC is tightly bound to FliGm in the default CCW state but this interaction is broken during a switch to CW rotation. The conformational change was identified by correlating the nature (CW or CCW bias) and position of rotationally biased mutants with conformational differences between two FliG crystal structures [20[••],36]. The involvement of helixMC in switching has since been supported by limited proteolysis experiments and the crystal structure of a CW-locked mutant [22]. Cooperative switching occurs as follows. Movement of HelixMC in one FliG protomer causes its adjacent FliG protomer to rotate. However, the construction of the ring ties adjacent FliGunits into the same orientation, with very little deviation allowed within stereochemical restraints. Consequently, rotation of one FliG protomer causes its neighbor to rotate and so on (Figure 3F and G). Thus, in contrast to Model A cooperativity is intrinsically built into the FliG ring. Moreover, Model B can accommodate the entire range of predicted motion of helixMC and subsequent rotation of all FliG protomers without violating stereochemical restraints [20[••]].

Model C

Switching in Model C also entails movement of helixMC [22]. However, this has not been developed into a molecular model. Conceptually, since helixMC is bound to its neighbor, cooperativity occurs via a similar mechanism to Model B where helixMC movement in one FliG protomer reorients its neighbor (Figure 3H, I).

Conclusions

Current models demonstrate that there are several possible molecular explanations for experimental data. This highlights the need for further characterization of the BFM to ultimately elucidate the molecular details of torque generation and switching. The strategies used to build these models provide an interesting example for modeling large molecular complexes in general from which several lessons can be learnt.

Model A was constructed with an intuitively logical strategy guided by all biochemical and EM experiments. Consequently such models will explain biochemical data well but one should keep in mind that biochemical data are used to build these models. Hence this agreement

should not be taken to prove that the models are necessarily correct since there is no independent validation. Nonetheless, this should allow models to continually evolve and be shaped by new data that will provide additional structural restraints until experiment and theory eventually converge or clash. The former occurs when there are no other likely or possible arrangements; the latter, when the model cannot reconcile divergent lines of evidence. Thus in data-driven model building it is imperative to recognize a clash and alter models accordingly to evolve with the most recent experiments.

The approach employed in the construction of Model B is perhaps less intuitive as it attempts to build a unifying model by only using high-resolution X-ray data, thereby ignoring most data that it should explain. One obvious potential flaw in this approach is that X-ray structures might not be physiologically relevant since they are determined from a crystal lattice; an argument raised by both the authors of model A and C. However, this strategy provides some distinct and powerful advantages. First, rather than being data driven, the model is in a sense blind to biochemical data and hence can be validated by its ability to explain experimental observations. For example Model B's fit with EM density, micrographs of the FliF–FliG fusion deletion mutant, correlation with cross-linking experiments and predictive model of the FliM ring and FliG–FliM contacts (Figure 3F, G and Figure 4) all constitute separate independent tests. Second, since X-ray structures provide atomic level pictures revealing not only how proteins are folded but also the precise molecular interactions responsible for its stability, they provide strict stereochemical restraints and in turn very well defined models where the key structural elements are either correct or not. These are not subject to change in light of new data. Rather, under the assumption that these key structural elements are correct, models are refined through experimental elucidation of any remaining degrees of freedom. The advantage of such well-defined models is that they make strong, experimentally falsifiable predictions that allow them to progress beyond data that were used to create them and thus providing tools to break new ground in our understanding of large molecular complexes.

References and recommended reading

Papers of particular interest, published within the annual period of review, have been highlighted as:

- • of special interest
- •• of outstanding interest

1. Thomas DR, Francis NR, Xu C, DeRosier DJ: **The three-dimensional structure of the flagellar rotor from a clockwise-locked mutant of Salmonella enterica serovar Typhimurium.** *Journal of Bacteriology* 2006, **188**:7039-7048.

2. Suzuki H, Yonekura K, Namba K: **Structure of the rotor of the bacterial flagellar motor revealed by electron cryomicroscopy and single-particle image analysis**. *Journal of Molecular Biology* 2004, **337**:105-113.

3. Minamino T, Imada K, Namba K: **Molecular motors of the bacterial flagella**. *Current Opinion in Structural Biology* 2008, **18**:693-701.

4. Sowa Y, Berry RM: **Bacterial flagellar motor**. *Quarterly Reviews of Biophysics* 2008, **41**:103-132.

5. Li H, Sourjik V: **Assembly and stability of flagellar motor in**
•• **Escherichia coli**. *Molecular Microbiology* 2011, **80**:886-899.
Fluorescensce microscopy based study on early BFM assembly that identifies FlhA within the export apparatus as the first substructure to form. In addition, studies of the turnover of proteins in the intact BFM support that FliF and FliG to form a stable core, while FliM and FliN are exchanged on timescales of 10–20 min.

6. Kojima S, Imada K, Sakuma M, Sudo Y, Kojima C, Minamino T, Homma M, Namba K: **Stator assembly and activation mechanism of the flagellar motor by the periplasmic region of MotB**. *Molecular Microbiology* 2009, **73**:710-718.

7. Roujeinikova A: **Crystal structure of the cell wall anchor domain of MotB, a stator component of the bacterial flagellar motor: implications for peptidoglycan recognition**. In *Proceedings of the National Academy of Sciences of the United States of America* 2008, **105**:10348-10353.

8. Yonekura K, Maki-Yonekura S, Homma M: **Structure of the**
• **flagellar motor protein complex PomAB: implications for the torque-generating conformation**. *Journal of Bacteriology* 2011, **193**:3863-3870.
First 3D structure of the isolated stator complex determined by electron microscopy that presumably captured the complex in a 'plugged' con-formation preventing ion leakage in the absence of load. A model of how the stator components generate torque is presented.

9. Li Z, Jensen GJ: **Electron cryotomography: a new view into microbial ultrastructure**. *Current Opinion in Microbiology* 2009, **12**:333-340.

10. Milne JL, Subramaniam S: **Cryo-electron tomography of bacteria: progress, challenges and future prospects**. *Nature Reviews. Microbiology* 2009, **7**:666-675.

11. Murphy GE, Leadbetter JR, Jensen GJ: **In situ structure of the complete Treponema primitia flagellar motor**. *Nature* 2006, **442**:1062-1064.

12. Kudryashev M, Cyrklaff M, Wallich R, Baumeister W,
• Frischknecht F: **Distinct in situ structures of the Borrelia flagellar motor**. *Journal of Structural Biology* 2010, **169**:54-61.
In situ visualization of the BFM in *Borrelia* spirochetes at 4.6 nm resolution using cryo-electron tomography. This study visualizes individual motor componenets and novel connections between stator and peptidoglycane and stator and rod structures. It also identifies two distinct species of BFM – one with and one without a switch complex. A novel mechanism for controlling the direction of rotation is suggested.

13. Liu J, Howell JK, Bradley SD, Zheng Y, Zhou ZH, Norris SJ:
• **Cellular architecture of Treponema pallidum: novel flagellum, periplasmic cone, and cell envelope as revealed by cryo electron tomography**. *Journal of Molecular Biology* 2010, **403**:546-561.
Cryo-electron tomography of intact *Treponema* spirochetes visualizing flagellar and other cellular componenets *in situ* and comparing them to *Borrelia* and *Salmonella* structures.

14. Liu J, Lin T, Botkin DJ, McCrum E, Winkler H, Norris SJ: **Intact flagellar motor of Borrelia burgdorferi revealed by cryo-electron tomography: evidence for stator ring curvature and rotor/C-ring assembly flexion**. *Journal of Bacteriology* 2009, **191**:5026-5036.

15. Lloyd SA, Tang H, Wang X, Billings S, Blair DF: **Torque generation in the flagellar motor of Escherichia coli: evidence of a direct role for FliG but not for FliM or FliN**. *Journal of Bacteriology* 1996, **178**:223-231.

16. Lloyd SA, Blair DF: **Charged residues of the rotor protein FliG essential for torque generation in the flagellar motor of Escherichia coli**. *Journal of Molecular Biology* 1997, **266**:733-744.

17. Yakushi T, Yang J, Fukuoka H, Homma M, Blair DF: **Roles of charged residues of rotor and stator in flagellar rotation: comparative study using H+-driven and Na+-driven motors in Escherichia coli**. *Journal of Bacteriology* 2006, **188**:1466-1472.

18. Zhou J, Blair DF: **Residues of the cytoplasmic domain of MotA essential for torque generation in the bacterial flagellar motor**. *Journal of Molecular Biology* 1997, **273**:428-439.

19. Zhou J, Lloyd SA, Blair DF: **Electrostatic interactions between rotor and stator in the bacterial flagellar motor**. In *Proceedings of the National Academy of Sciences of the United States of America* 1998, **95**:6436-6441.

20. Lee LK, Ginsburg MA, Crovace C, Donohoe M, Stock D: **Structure**
•• **of the torque ring of the flagellar motor and the molecular basis for rotational switching**. *Nature* 2010, **466**:996-1000.
Crystal structure of full-length FliG from *Aquifex aeolicus* showing three distinct globular domains separated by two long helices. Conformational differences between crystal structures and conserved crystal contacts are used to build a model of the switch complex and suggest a molecular mechanism for rotational switching.

21. Lloyd SA, Whitby FG, Blair DF, Hill CP: **Structure of the C-terminal domain of FliG, a component of the rotor in the bacterial flagellar motor**. *Nature* 1999, **400**:472-475.

22. Minamino T, Imada K, Kinoshita M, Nakamura S, Morimoto YV, Namba K: **Structural insight into the rotational switching mechanism of the bacterial flagellar motor**. *PLoS Biology* 2011, **9**:e1000616.

23. Paul K, Brunstetter D, Titen S, Blair DF: **A molecular mechanism**
•• **of direction switching in the flagellar motor of Escherichia coli**. In *Proceedings of the National Academy of Sciences of the United States of America* 2011, **108**:17171-17176.
Mutational and cross-linking studies suggesting a molecular mechanism of BFM switching that is triggered by phospho-CheY binding to the lower part of the switch complex where it induces a tilt in FliM resulting in a 90° rotation of FliGc leading to motor reversal.

24. Francis NR, Sosinsky GE, Thomas D, DeRosier DJ: **Isolation, characterization and structure of bacterial flagellar motors containing the switch complex**. *Journal of Molecular Biology* 1994, **235**:1261-1270.

25. Francis NR, Irikura VM, Yamaguchi S, DeRosier DJ, Macnab RM: **Localization of the Salmonella typhimurium flagellar switch protein FliG to the cytoplasmic M-ring face of the basal body**. In *Proceedings of the National Academy of Sciences of the United States of America* 1992, **89**:6304-6308.

26. Porter SL, Wadhams GH, Armitage JP: **Signal processing in**
• **complex chemotaxis pathways**. *Nature Reviews. Microbiology* 2011, **9**:153-165.
Comprehensive review of bacterial chemotaxis.

27. Brown MT, Delalez NJ, Armitage JP: **Protein dynamics and**
• **mechanisms controlling the rotational behaviour of the bacterial flagellar motor**. *Current Opinion in Microbiology* 2011.
Up-to-date review of BFM subunit turnover and novel control mechanisms.

28. Bai F, Branch RW, Nicolau DV Jr, Pilizota T, Steel BC, Maini PK, Berry RM: **Conformational spread as a mechanism for cooperativity in the bacterial flagellar switch**. *Science* 2010, **327**:685-689.

29. Duke TA, Bray D: **Heightened sensitivity of a lattice of membrane receptors**. In *Proceedings of the National Academy of Sciences of the United States of America* 1999, **96**:10104-10108.

30. Cluzel P, Surette M, Leibler S: **An ultrasensitive bacterial motor revealed by monitoring signaling proteins in single cells**. *Science* 2000, **287**:1652-1655.

31. Sourjik V, Berg HC: **Binding of the Escherichia coli response regulator CheY to its target measured in vivo by fluorescence resonance energy transfer**. In *Proceedings of the National Academy of Sciences of the United States of America* 2002, **99**:12669-12674.

32. Nakamura S, Kami-ike N, Yokota JP, Minamino T, Namba K:
•• **Evidence for symmetry in the elementary process of bidirectional torque generation by the bacterial flagellar motor**. In *Proceedings of the National Academy of Sciences of the United States of America* 2010, **107**:17616-17620.

Single molecule analysis of Salmonella BFMs at high spatial and temporal resolution showing that there are 26 equal steps per 360° rotation in either direction. The symmetrical behavior of switching suggests a 180° rotation of the FliGc domain involved in torque generation. This is in contrast to an earlier study of a sodium dependent BFM that showed different steps for CCW and CW rotaion.

33. Sowa Y, Rowe AD, Leake MC, Yakushi T, Homma M, Ishijima A, Berry RM: **Direct observation of steps in rotation of the bacterial flagellar motor**. *Nature* 2005, **437**:916-919.

34. Young HS, Dang H, Lai Y, DeRosier DJ, Khan S: **Variable symmetry in Salmonella typhimurium flagellar motors**. *Biophysical Journal* 2003, **84**:571-577.

35. Chen SY, Beeby M, Murphy GE, Leadbetter JR, Hendrixson DR,
•• Briegel A, Li Z, Shi J, Tocheva EI, Muller A *et al.*: **Structural diversity of bacterial flagellar motors**. *The EMBO Journal* 2011, **30**:2972-2981.
In situ cryo-electron tomography survey of BFMs across a variety of bacteria showing that the structure of the BFM is anything but conserved. The structural diversity of different BFMs seen in this study puts a word of caution on the current attempts to derive unified molecular models for flagellar motor architecture and switching.

36. Brown PN, Hill CP, Blair DF: **Crystal structure of the middle and C-terminal domains of the flagellar rotor protein FliG**. *The EMBO Journal* 2002, **21**:3225-3234.

37. Brown PN, Mathews MA, Joss LA, Hill CP, Blair DF: **Crystal structure of the flagellar rotor protein FliN from Thermotoga maritima**. *Journal of Bacteriology* 2005, **187**:2890-2902.

38. Park SY, Lowder B, Bilwes AM, Blair DF, Crane BR: **Structure of FliM provides insight into assembly of the switch complex in the bacterial flagella motor**. In *Proceedings of the National Academy of Sciences of the United States of America* 2006, **103**:11886-11891.

39. Paul K, Gonzalez-Bonet G, Bilwes AM, Crane BR, Blair D:
•• **Architecture of the flagellar rotor**. *The EMBO Journal* 2011, **30**:2962-2971.
Crystal structure of a FliGm–FliMm complex from *T. maritima* in combination with biochemical and cross-linking studies suggest a model for the assembly of the entire switch complex and offers a possible explanation to the symmetry mismatch between MS (∼26-fold symmetry) and C (∼34-fold symmetry) rings.

40. Brown PN, Terrazas M, Paul K, Blair DF: **Mutational analysis of the flagellar protein FliG: sites of interaction with FliM and implications for organization of the switch complex**. *Journal of Bacteriology* 2007, **189**:305-312.

41. Lowder BJ, Duyvesteyn MD, Blair DF: **FliG subunit arrangement in the flagellar rotor probed by targeted cross-linking**. *Journal of Bacteriology* 2005, **187**:5640-5647.

42. Sarkar MK, Paul K, Blair DF: **Subunit organization and reversal-
• associated movements in the flagellar switch of Escherichia coli**. *The Journal of Biological Chemistry* 2010, **285**:675-684.
Cross-linking studies of FliMc and FliN establishing a molecular model of their interaction and of the lower part of the switch complex.

43. Sarkar MK, Paul K, Blair D: **Chemotaxis signaling protein CheY
•• binds to the rotor protein FliN to control the direction of flagellar rotation in Escherichia coli**. In *Proceedings of the National Academy of Sciences of the United States of America* 2010, **107**:9370-9375.
Mutagenesis and biochemical cross-linking studies that show that phospho-CheY not only binds to the N-terminus of FliM, but that the switch to CW rotation also involves interaction of phospho CheY with FliN. A molecular model for rotaional switching involving FliN is provided.

44. Marykwas DL, Berg HC: **A mutational analysis of the interaction between FliG and FliM, two components of the flagellar motor of Escherichia coli**. *Journal of Bacteriology* 1996, **178**:1289-1294.

45. Passmore SE, Meas R, Marykwas DL: **Analysis of the FliM/FliG motor protein interaction by two-hybrid mutation suppression analysis**. *Microbiology* 2008, **154**:714-724.

46. Thomas D, Morgan DG, DeRosier DJ: **Structures of bacterial flagellar motors from two FliF–FliG gene fusion mutants**. *Journal of Bacteriology* 2001, **183**:6404-6412.

47. Andrade MA, Petosa C, O'Donoghue SI, Muller CW, Bork P: **Comparison of ARM and HEAT protein repeats**. *Journal of Molecular Biology* 2001, **309**:1-18.

48. Tewari R, Bailes E, Bunting KA, Coates JC: **Armadillo-repeat
• protein functions: questions for little creatures**. *Trends in Cell Biology* 2010, **20**:470-481.
Review of armadillo repeat proteins and their diverse and versatile functions in eukaryotes.